



**ESTEC**

European Space Research  
and Technology Centre  
Keplerlaan 1  
2201 AZ Noordwijk  
The Netherlands  
[www.esa.int](http://www.esa.int)

# PERFORMANCE REPORT

## Assessing the Impact of the MSA Leakage on IFU Observations

<b>Prepared by</b>	<b>A. Deshpande</b>
<b>Reference</b>	<b>ESA-JWST-SCI-NRS-RP-2017-002</b>
<b>Issue/Revision</b>	<b>1.0</b>
<b>Date of Issue</b>	<b>February 28, 2018</b>
<b>Status</b>	<b>Draft</b>



# APPROVAL

<b>Title</b> Assessing the Impact of the MSA Leakage on IFU Observations	
<b>Issue Number</b> 1	<b>Revision Number</b> 0
<b>Author</b> A. Deshpande	<b>Date</b> February 28, 2018
<b>Approved by</b> the boss	<b>Date of Approval</b> whenever

# CHANGE LOG

Reason for change	Issue Nr.	Revision Number	Date

# CHANGE RECORD

<b>Issue Number</b> 1	<b>Revision Number</b> 0		
Reason for change	Date	Pages	Paragraph(s)

# DISTRIBUTION

Name/Organisational Unit
SCI-ODJ
SCI-S
STScI
ESTEC



## Contents

<b>1</b>	<b>Introduction</b>	<b>4</b>
<b>2</b>	<b>Determining Leakage Statistics</b>	<b>4</b>
2.1	Selecting Exposures	4
2.2	Quantifying the Impact	6
2.3	Cleaning the Data	6
2.4	Estimating the Expected Leakage Background Level	7
2.5	Modeling the Leakage in 1D	8
<b>3</b>	<b>Interpreting Leakage Statistics</b>	<b>9</b>
3.1	The Medium Resolution Gratings	9
3.2	The High Resolution Gratings	12
3.3	The Prism	15
3.4	Simulating the Impact of Zodiacal Light	17
<b>4</b>	<b>Evaluating the Impact On an Observation</b>	<b>19</b>
<b>5</b>	<b>Conclusion</b>	<b>21</b>
<b>6</b>	<b>References</b>	<b>22</b>

## 1 INTRODUCTION

The Near Infrared Spectrograph (NIRSpec) instrument is one of the four scientific instruments aboard the James Webb Space Telescope (JWST). The instrument possesses several operational modes; Multi-Object Spectroscopy (MOS), Fixed Slit spectroscopy (FS), and Integral Field Spectroscopy (IFS). NIRSpec makes use of a variety of filters and dispersive elements to obtain spectra across a range of different wavelengths. Their basic characteristics are listed in NTN-2013-011 (Giardino 2013). As a consequence of their spectra sharing the same detector space, observations from the MOS and IFS modes must be, generally speaking, mutually exclusive. Consequently, the Micro-Shutter Assembly (MSA), used for MOS, must be fully closed when using the Integral Field Unit (IFU).

However, there is some amount of light passing through the MSA even when fully closed, which affects IFU observations. Part of this is explained by the existence of Failed Open (FO) shutters; defective shutters that are permanently open. There also exists a more subtle effect common to all shutters, that creates the parasitic signal referred to here as ‘MSA leakage’. This occurs due to the MSA’s finite, non-ideal contrast. These effects are illustrated in Figure 1. The origins of the MSA leakage, together with initial attempts at modeling it in imaging mode, are detailed within ESA-JWST-SCI-NRS-TN-2017-051 (Lützgendorf 2017). While it is a straightforward process to identify and flag the FO signal, the ‘leakage’ proves more complex due to its pervasiveness and spatial variability. Therefore, it becomes necessary to assess its precise impact on IFU observations, in order to assist in any modeling and compensation attempts.

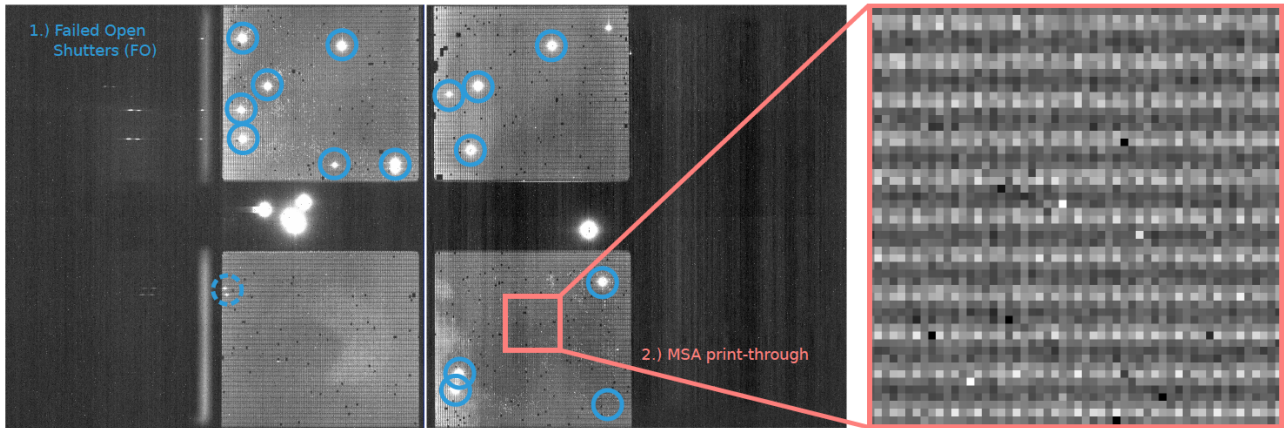
In this document we set out to quantify, down to the pixel level, how this parasitic signal compares to the direct IFS spectrum of the diffuse, extended ‘background’ source causing it. During on-sky observations, this ‘background’ source will typically be the Zodiacal light while, on the ground, we used NIRSpec’s internal calibration source. This source provides a uniform illumination over the complete field of view. The data presented here attempts to represent the relative importance of the parasitic signal compared to the Zodiacal light. The following sections describe the techniques, computational tools and exposures used in order to quantify this parasitic signal, and the statistics obtained as a result.

## 2 DETERMINING LEAKAGE STATISTICS

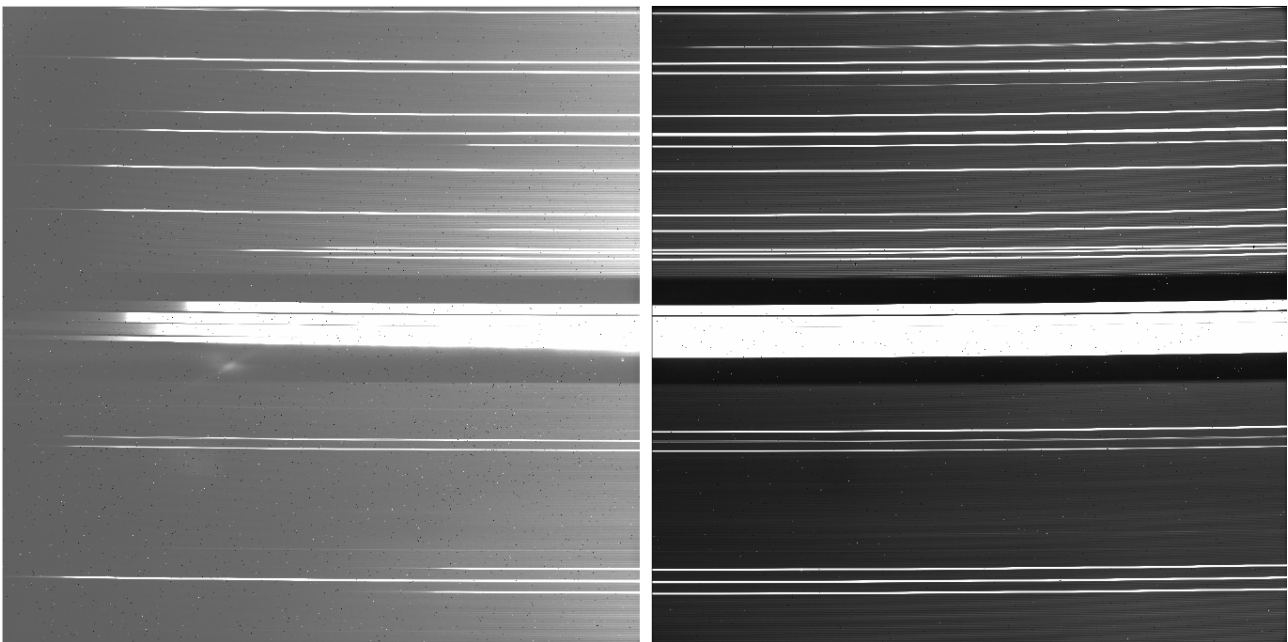
### 2.1 Selecting Exposures

For a given source, it is possible to image the ‘MSA Leakage’ by closing both the operable MSA shutters and the IFU aperture. By comparing these ‘background’ exposures to the exposures obtained for the object with the IFU aperture open, the impact of the leakage on observations can be assessed. NIRSpec contains a Calibration Assembly (CAA) which is equipped with a series of lamps; each corresponding to how a uniform external source would appear when viewed through a specific filter. In cryo-vacuum ground testing, exposures were obtained with these lamps in both IFU open and closed configurations. The NIDs of these observations, together with their respective filter and element combinations, wavelength ranges, and the CAA lamps used are given in Table 1.

By utilising the NIRSpec Instrument Pipeline Software (NIPS) (Dorner 2012) with the observations listed above, the impact of the MSA leakage on IFU observations was explored at electron count-rate map, 2D irregular, and data-cube level. The count-rate map was accessed using the standard NIPS pipeline code, ‘pipelineIPS.py’, whereas the 2D irregular spectra and cubes were generated using ‘p\_getCubeIFU.py’. In all cases the ‘ISIM’ environment was fed into the instrument model.



(a) The parasitic signal seen in imaging mode. This exposure was obtained for configuration MSA=ALLCLOSED, IFU=closed with the internal FLAT lamp. The blue circles highlight FO shutters, whereas the remaining pattern is the leakage. The bright circles in the central region is light from the apertures for the instrument’s fixed slits. (Lützgendorf 2017)



(b) When obtaining spectra, this parasitic signal propagates and piles up in the spectral dimension, as shown in this figure. This is ISIM NID 30197 for configuration G140M, MSA=ALLCLOSED, IFU=closed, with lamp FLAT1. This lamp is equivalent to an extended source viewed through F100LP. Again, two distinct features are observed: the bright, pronounced isolated white lines which are signal from individual FO shutters; and the more nebulous, lower magnitude MSA leakage. Similar to 1a, the thick spectra in the central region are from the instrument’s fixed slits.

Figure 1: Exposures illustrating the parasitic signal known as MSA leakage in imaging and spectral modes.

**Table 1: List of calibration observation NIDs for all instrument configurations used in MSA leakage assessment. Note: The NIDs listed here are all for the 'ISIM' environment. Additionally, while the operational range for the two FLAT4 configurations is, in principle, from 0.7  $\mu\text{m}$ , the IFU in fact truncates the spectra at the values listed in the brackets. Similarly, for the Prism configuration the intensity of the FLAT5 lamp drops off drastically below the value listed in the brackets, resulting in essentially no signal. Correspondingly, the impact of the leakage also cannot be examined below this point.**

Disperser	Equivalent Filter	CAA Lamp	IFU Open NID	IFU Closed NID	Wavelength Range ( $\mu\text{m}$ )
G140M	F070LP	FLAT4	30191	30196	0.7 (0.92) - 1.2
G140M	F100LP	FLAT1	30190	30197	1.0 - 1.8
G140H	F070LP	FLAT4	30076	30083	0.7 (0.95) - 1.2
G140H	F100LP	FLAT1	30075	30086	1.0 - 1.8
G235M	F170LP	FLAT2	30226	30234	1.7 - 3.1
G235H	F170LP	FLAT2	30113	30124	1.7 - 3.1
G395M	F290LP	FLAT3	30272	30278	2.9 - 5.2
G395H	F290LP	FLAT3	30152	30161	2.9 - 5.2
PRISM	CLEAR	FLAT5	30340	30362	0.6 (0.75) - 5.3

## 2.2 Quantifying the Impact

For the purposes of the investigation, the metric of the impact of the parasitic signal on any given observation datum was determined to be the leakage level as a percentage of the direct background spectrum signal at a given pixel. At count-rate and 2D irregular levels, the IFU closed exposure was divided pixel-wise by the result of subtracting the IFU closed exposure from its IFU open counterpart. Finally, to obtain the percentage, these quantities were multiplied by 100. A similar process was employed at cube level, but now applied to every cell within the cube. So, the percentage impact at data-point  $i$ ,  $P_i$ , is given by:

$$P_i = \frac{C_i}{O_i - C_i} \times 100, \quad (1)$$

where  $C_i$  and  $O_i$  are the IFU closed and open values at point  $i$ , respectively.

## 2.3 Cleaning the Data

As a first step in being able to precisely assess the impact of the MSA leakage, it was necessary to mask the contribution of FO spectra. The already known location of the FO shutters in MSA coordinates was extracted from the map file 'nrs\_msa1\_CHK\_20151211.ms1' by isolating those with the appropriate flag. The spectral pixel coordinates corresponding to their leakage were determined by passing their MSA coordinates through the NIPS function 'm\_cutSlitTrace'; producing windows containing the spectra of each shutter. This was done for each CAA/Disperser combination to ensure proper coverage, and the data at the coordinates contained within these windows was then masked.

Furthermore, another element requiring masking within the observation was 'bad pixels'; i.e corrupted pixels that had either negative or arbitrarily large values. The former was accomplished by simply creating a mask for any data points with a value less than zero. The latter was accomplished primarily using the quality flags found within the FITS files of the exposures. However, these flags proved incomplete. Inspection revealed the presence of clearly corrupted pixels that were not masked. In order to ensure complete coverage of this 'bad' data, the statistically robust 'modified Z-score' criterion for outlier detection (Iglewicz & Hoaglin 1993) was used. Any data points with values,  $x_i$ , that satisfied:

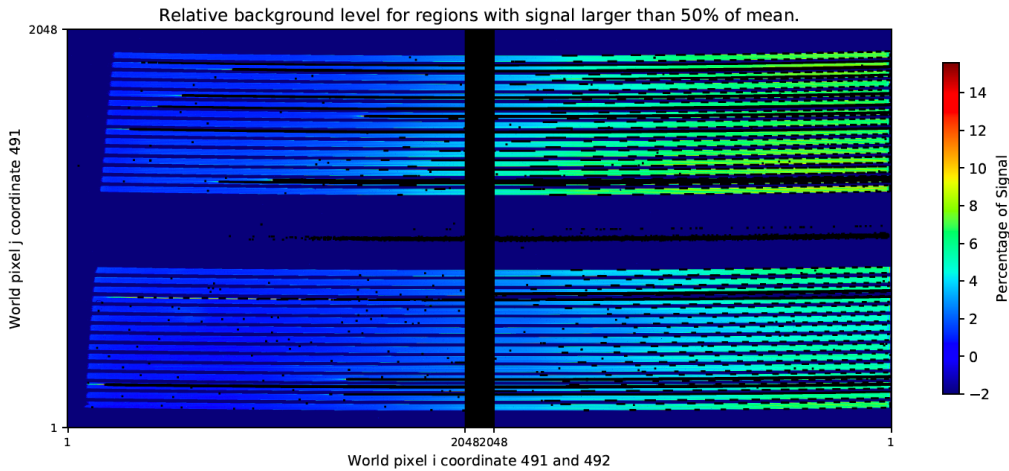


Figure 2: ‘MSA Leakage’ as a percentage of signal per pixel for grating G140H, CAA lamp FLAT1 (equivalent to filter F100LP). Pixels in black are masked regions due to FO shutters or bad pixels. Pixels with values less than half of the mean in the background-subtracted map are set to -2.

$$x_i > \tilde{x} + \frac{3.5 \times MAD}{0.6745}, \tag{2}$$

where  $\tilde{x}$  is the median of the data, and the  $MAD$  is the median absolute deviation, were masked. This additional step of masking was not applied to the Prism configuration, since its large dynamic range leads to data with relevant signal being cast as outliers, and ignored. Instead a simple sanity check was instituted to mask any pixels with values greater than or equal to 1000%. Similarly, the ‘Z-score’ technique results in over-masking in the 4.5 - 5.2  $\mu\text{m}$  range for the G395M and G395H configurations. For these, the remaining offending pixels were manually identified and masked, in both cases being due to a not wholly covered feature in Slice 4.

The regions of the exposure cut by the ‘p\_getCubeIFU.py’ method for each IFU slice also contained areas without signal on their periphery. As a final step, these regions were also masked; in order to ensure they had no impact on the desired statistics. Any pixels within the 2.5% of the slice above the spectrum, and within the 2.5% of the slice below the spectrum, were masked. This was done using the ‘slity’ extension generated by NIPS for each pixel. Points with fractions beyond  $\pm 0.475$  were masked.

## 2.4 Estimating the Expected Leakage Background Level

The count-rate map level was explored purely for illustration purposes, and to build intuition for the change in leakage across the detectors. All pixels which, in the background-subtracted map, have values less than 50% of its mean were identified. Within the percentage difference maps, these pixels were set to an arbitrarily low negative value. This was done in order to ensure that only regions with signal were being considered. Plots were generated showing the percentage difference across the data. An example of the visualisations explored at count-rate map level is shown above, in Figure 2. These visualisations do not provide great quantitative detail. Therefore, it is of more use to report directly the statistics obtained and histograms of the leakage.

However, the ideal stage to carry out statistical analysis was determined to be the 2D irregular spectrum level. Here, the spectral trace for each slice has been individually identified and extracted. Additionally, it is superior to the cube level, because the interpolation and additional processing done when generating the cube may obscure the features of the leakage. For this level, the means, medians, standard deviations, and MADs were

calculated for the two detector Sensor Chip Arrays (SCAs) individually, as well as the data set as a whole. These were determined for the data both before and after applying the masking described previously. Without masking, the presence of the 'bad' pixels and FO shutters leads to large standard deviations and poorly representative means. It is for this reason the more statistically robust MAD was also calculated. It also meant the median is a better representation for these data than the mean. Histograms, each of 1000 bins, were also created showing the range of percentage difference values, after masking, for each instrument configuration. To complement these, cumulative histograms were plotted on the same axis, and the 95<sup>th</sup> percentile was computed for each configuration. Since the final masking criterion could not be applied for the Prism, and G395 configurations, there remained within this data pixels with arbitrarily high values. Visually, these would bias the histogram such that it becomes a poor representation of the distribution of leakage. To correct for this, the histogram was clipped when values on the frequency axis reached 1% of their peak. Values in the remaining range were then re-binned into 1000 bins.

In order to better understand the structure of the leakage, an analysis was also carried out of how it varies across wavelength for each configuration. Specifically, the change of the median leakage percentage with wavelength was charted. Firstly, the FO and bad data was masked using the previously described process. Next, across each configuration's wavelength range, 20 evenly spaced wavelengths were chosen. All parasitic signal values, from across all of the slices, at wavelengths matching these to three decimal places were collected. The median leakage value was then computed for each wavelength individually. Scatter plots were then generated showing the change of the median with wavelength. Pseudo error bars were added to these graphs, in order to account for the spatial variation of leakage at each given wavelength. For the lower bound, the minimum percentage value at each wavelength was used. However, in order to provide an effective upper bound without just hitting the limit of masking, the standard deviation ( $\sigma$ ) of values was used. In particular, the upper bound was chosen as the  $3\sigma$  level.

## 2.5 Modeling the Leakage in 1D

The spectra of the FLAT CAA lamps used for the purpose of the investigation discussed in the previous section are not, in fact, flat. Therefore, in order to accurately work out how the percentage of leakage changes with the Zodiacal light, it was necessary to account for the differences in their spectra. This would be achieved by constructing a one-dimensional model of the the IFS and MOS signals for a given IFU slice, for each configuration. For a selected configuration, the model would first compute the wavelength ranges for the zeroth, -1, and -2 orders for the MOS signal, as well as the -1 order for the IFS signal. Using `nirspecperf.py`, it would also compute the Photon Conversion Efficiency (PCE) for each of the aforementioned orders. The model would next take an input spectrum, and contain it in an instance of the `Spectrum` class from `spectrum.py`. The various orders for these spectra were calculated, and then re-binned into the pixel resolution of the detector. Finally, they were converted into electron rates by using the PCEs.

Next, a boolean list was generated with a length matching the number of pixels of the detector's j-axis. Using the `'NRS42'` radiometric model and the `'NIRS_FM2_05_CV3_FIT1'` geometrical model, the extent in detector pixels covered by a given wavelength of light incident on an entire row of MSA quadrants 1 and 3 was determined. Starting from the zeroth index of the list, indices within this extent were assigned a value of one. For this purpose, the 85 row of the two quadrants is used; a purely arbitrary selection. This list was then convolved, independently, with the -1 and -2 orders of the MOS spectra, in order to approximate the distribution of leakage in the detector's spectral direction. Multiple separate arrays were then generated, one for each of the MOS orders and one for the IFS order, again with a length matching the detector's j-axis. Again selecting the 85th row, and by using the geometric and radiometric models, the starting positions of the -1 and -2 MOS orders of leakage on the detector were calculated. For this, the lowest wavelength in the order was fed through first shutter of the row in quadrant 3. Each of the convolved leakage distributions were then placed in one of the arrays, with an initial index corresponding to that order's start position. A slightly different procedure was employed for the zeroth order. Initially, the detector j-coordinate for an arbitrary wavelength passing through the final shutter in quadrant 1 was calculated. Simultaneously, the zeroth order MOS electron rate spectrum was summed over. This value was assigned to all of the zeroth order array indices, up-to and including the previously calculated

j-coordinate. Similarly, the relevant IFS order was placed into its array at the corresponding start point of its spectrum. In this case, the fifth IFU slice was selected for propagation through the instrument models, as this approximately matched the spatial region of the detector where the simulated MOS spectra would fall. Finally, for the same IFU slice, the detector coordinates for the science wavelength range of the current configuration were calculated. In the case of the PRISM, only the zeroth orders were considered in the above procedure.

The model's ultimate purpose was to successfully reproduce the observed MSA leakage. This was accomplished by taking the ratio of the simulated parasitic light signal to the simulated IFS signal, over the determined science indices. Graphs were plotted charting this ratio across the science range. However, the multiplication of an additional factor by the IFS spectrum was required within this calculation, to account for the contrast of the leakage to the IFS signal. This contrast was determined by inspection and trial-and-error, through comparing the model to the statistics determined from observation. Additionally, this matching process revealed that the zeroth order impact was being over-estimated by the model. A supplementary factor of 0.05 was consequently applied to the magnitude of the zeroth order MOS signal; leading to an optimal match.

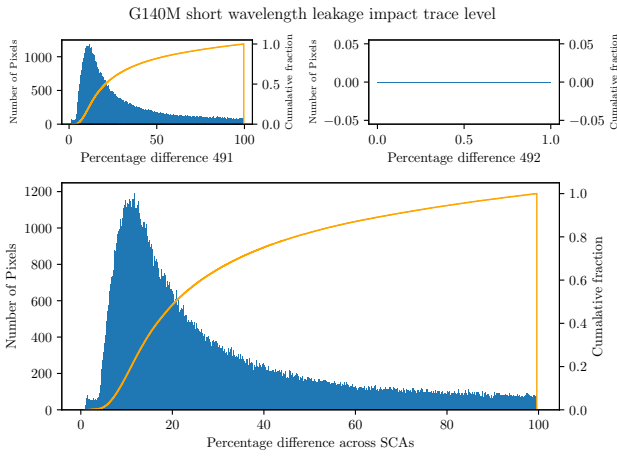
### 3 INTERPRETING LEAKAGE STATISTICS

#### 3.1 The Medium Resolution Gratings

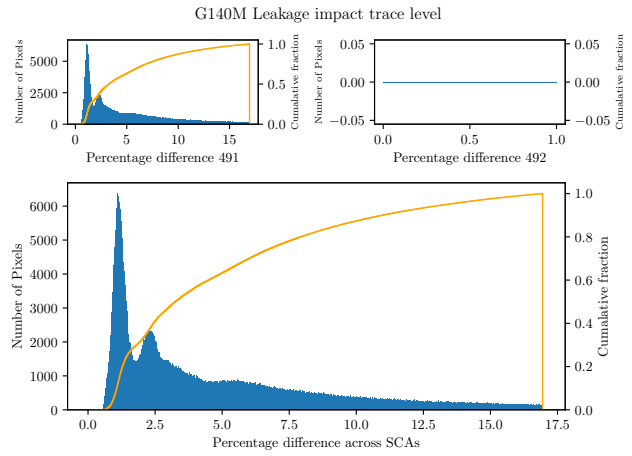
The statistics obtained for the medium resolution, or 'M' gratings, are stated below, in Table 2. The corresponding histograms are given in Figure 3. Plots showing how the median percentage of leakage changes with wavelength for these configurations are presented in Figure 4. Also shown in this figure are the results of the 1D model. The graphs are designed to display the individual parasitic signal distributions for SCA491 and SCA492, as well as both together. However, for the Medium resolution gratings, none of diffraction order -1 falls on SCA492. Accordingly, there is no contribution to the statistics from SCA492. In general, the majority of the signal is < 10% of the incident source spectra intensity. In the case of G140M, shown in Figures 4a and 4b, the leakage decreases with wavelength. This trend can be attributed to a confluence of two effects. Part of it can be explained as a consequence of the zeroth order of diffraction also falling on the detector. Examining Figure 4b closely, a consistent level of median between 1.2 and 1.4  $\mu\text{m}$ , followed by a sharp drop, can be observed. This is the imprint of the zeroth order. Complementing this, the rapid increase in leakage as wavelength decreases, prior to 1.2  $\mu\text{m}$  is due to the spectrum of the CAA lamp dropping off. Similarly, for Figure 4a, the heightened level of parasitic signal is attributable to order -1 being located wholly within the zeroth order imprint region of the detector. Once again, the observed trend is due to spectrum dropping off at the lower wavelengths. In fact, this effect is present for all of the medium resolution gratings. However, the effect is most pronounced in the G140M band because the zeroth order is dominated by the red light, resulting in the zeroth order being significantly more intense than order -1 over the relevant range.

**Table 2: Averages and measures of spread for 'M' grating configurations, before (BM) and after (AM) applying masking. The 95<sup>th</sup> percentile is given after masking. All values are background as a percentage of signal. The asterisked G395M row contains the statistics obtained when the configuration is cut off at 4.5 $\mu\text{m}$ .**

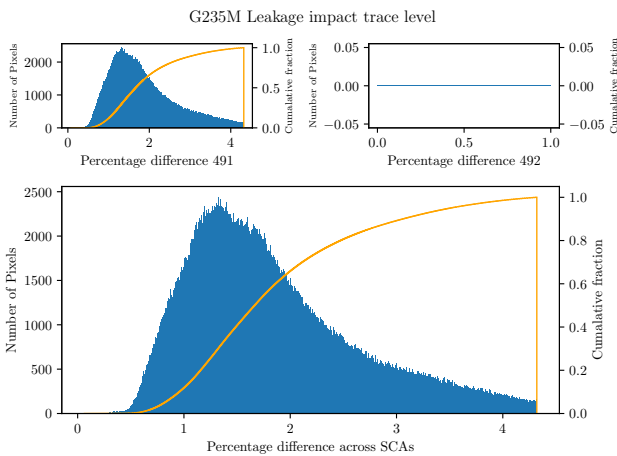
Disperser	Filter	Mean		Median		Standard Deviation		MAD		95 <sup>th</sup> Percentile
		BM	AM	BM	AM	BM	AM	BM	AM	
G140M	F070LP	2633.02	29.43	47.36	20.72	105280.23	23.08	37.07	10.52	81.69
G140M	F100LP	966.52	4.75	9.56	3.26	94768.07	3.96	8.34	2.07	13.38
G235M	F170LP	542.23	1.84	2.58	1.67	39267.90	0.81	1.45	0.49	3.51
G395M	F290LP	1442.32	1.84	6.34	1.14	464160.29	1.82	5.93	0.71	6.63
G395M*	F290LP	357.89	1.23	1.90	0.94	15332.11	0.90	1.46	0.53	3.14



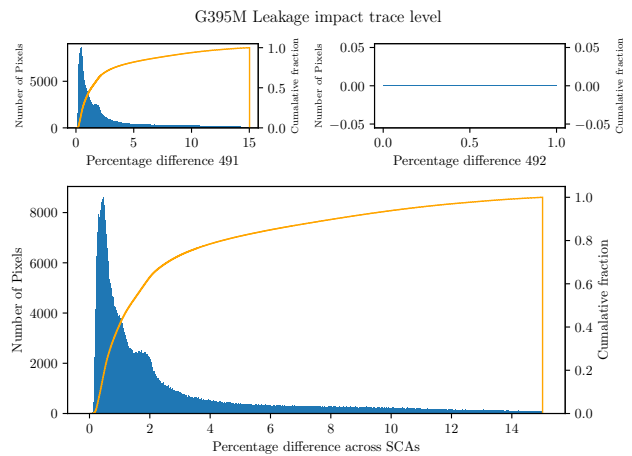
(a) G140M between 0.92 & 1.2  $\mu\text{m}$ .



(b) G140M between 1.0 & 1.8  $\mu\text{m}$ .



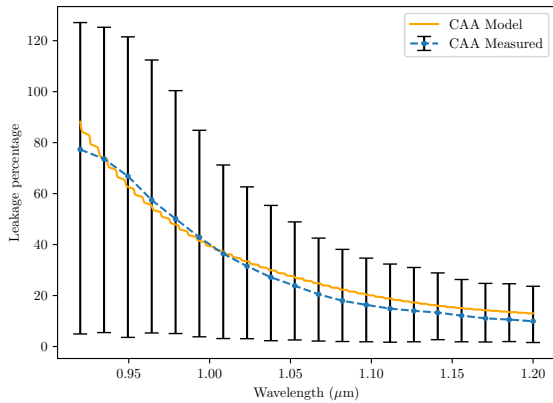
(c) G235M between 1.7 & 3.1  $\mu\text{m}$ .



(d) G395M between 2.9 & 5.2  $\mu\text{m}$ .

Figure 3: Histograms showing the distribution of MSA leakage as a percentage of the signal per pixel, for the 'M' gratings, in blue. In orange are the cumulative histograms for the same data. In each case 1000 bins were used. The leakage across SCAs 491 and 492 are shown individually, and then together.

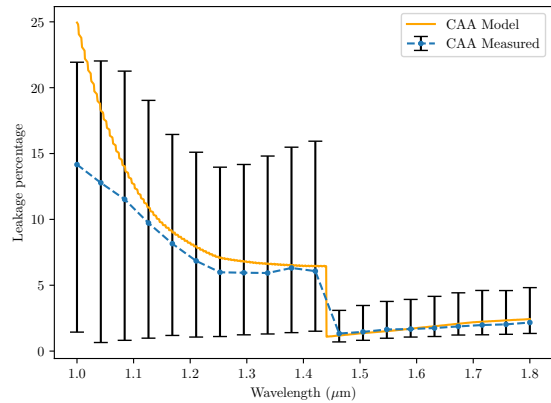
G140M F070LP Leakage Data-Model Comparison



Approx. best contrast: 3500

(a) G140M between 0.92 & 1.2  $\mu\text{m}$ .

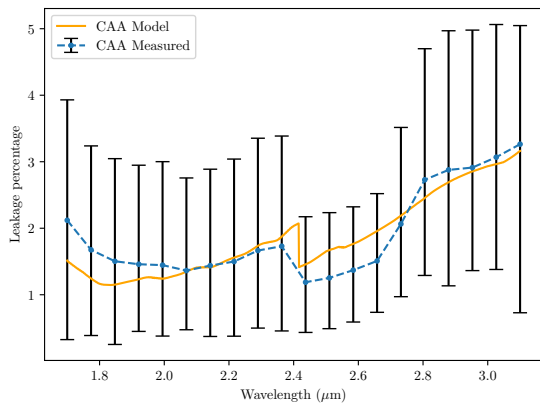
G140M F100LP Leakage Data-Model Comparison



Approx. best contrast: 5500

(b) G140M between 1.0 & 1.8  $\mu\text{m}$ .

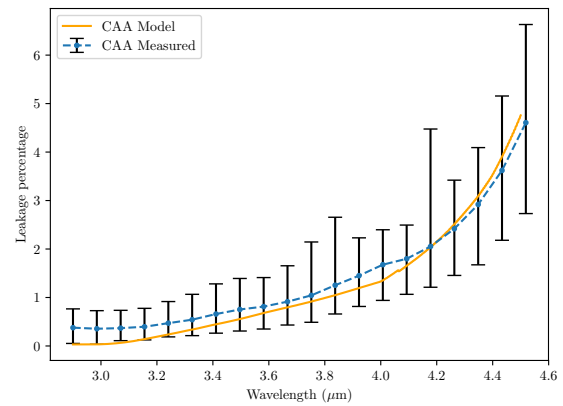
G235M F170LP Leakage Data-Model Comparison



Approx. best contrast: 4000

(c) G235M between 1.7 & 3.1  $\mu\text{m}$ .

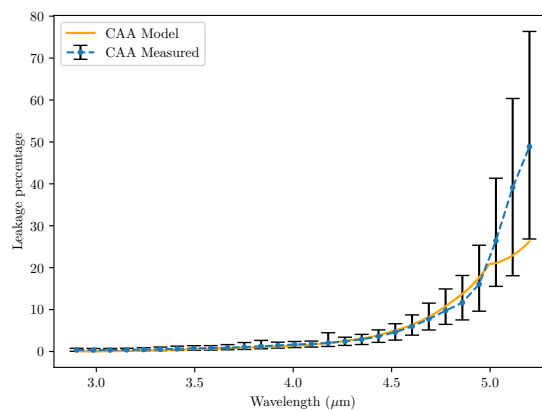
G395M F290LP Leakage Data-Model Comparison



Approx. best contrast: 4000

(d) G395M between 2.9 & 4.5  $\mu\text{m}$ .

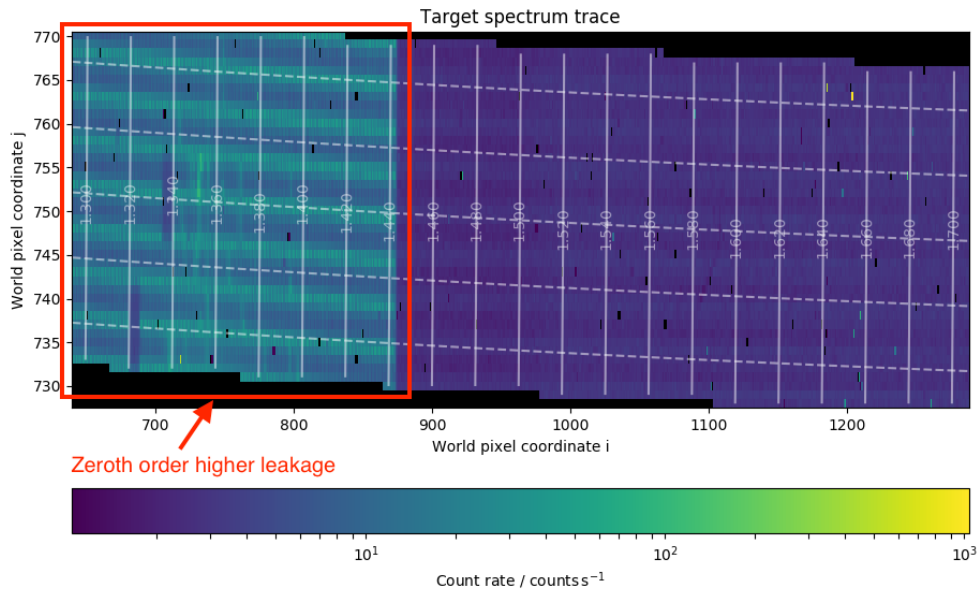
G395M F290LP Leakage Data-Model Comparison



Approx. best contrast: 4000

(e) G395M between 2.9 & 5.2  $\mu\text{m}$ .

Figure 4: Change of the median of leakage as a percentage of signal, with wavelength, for ‘M’ dispersers; observed and modeled. Each scatter plot consists of 20 points, evenly spaced across the disperser’s wavelength range. The pseudo error bars, in black, describe the spatial spread of leakage at a wavelength. The lower bound is the minimum value at that wavelength, while the upper bound extends to  $3\sigma$  above. The ‘approximate contrast’ refers to the relative contrast used within the model of MOS spectra to IFS spectra.



SMOS-MOD-G1M-21-5344181719\_30197\_JLAB88\_JW1  
 Mode: IFU, slice 2, OPAQUE, G140M

**Figure 5:** 2D Irregular view of NID 30197, which shows the ‘background’ for the G140M, FLAT1 configuration. This is the third of the IFU slices, and a similar pattern is observed across each of the slices. A distinct demarcation of regions is observed, with the highlighted part having higher values due to the imprint of the zeroth order of diffraction. A similar effect is present in all the ‘M’ configurations.

For G235M and G395M, the orders are more comparable. Consequently, the effect’s impact is less noticeable for G235M, and not at all obvious for G395M. An example of the zeroth order imprint is illustrated in Figure 5. On the other hand, for G235M and G395M, the median of the parasitic signal increases with wavelength. This is due to the leakage piling up in the detector *i* coordinate and the spectrum of the CAA lamp dropping again at higher wavelengths. The drastic increase in relative impact for G395M beyond 4.5  $\mu\text{m}$  is a particularly egregious example of lamp spectrum effect. This in turn also has a large effect on the statistics of the configurations. Accordingly, statistics are provided for these both with and without a cut-off at 4.5  $\mu\text{m}$ . Both data sets are included, to provide a realistic idea of the parasitic signal experienced, in case an observation is not concerned with the 4.5 - 5.2  $\mu\text{m}$  range. The 1D model also appears to be largely consistent with the observed data, with the exception being the G395 configuration. The deviation of the model here at higher wavelengths can be explained by the fact that the input spectrum used to represent CAA FLAT 3. The spectrum is poorly interpolated at its higher wavelength end, meaning it is a sub-par representation of the true lamp spectrum at the extremes. In fact, this is true of all configurations, but is particularly egregious for FLAT 3.

### 3.2 The High Resolution Gratings

The statistics obtained for the high resolution, or ‘H’ gratings, are stated below, in Table 3. The corresponding histograms are given in Figure 6. The graphs display the individual parasitic signal distributions for SCA491 and SCA492 (where appropriate), as well as both together. In general, the majority of the leakage is < 10% of the total signal. Plots showing how the median percentage of leakage changes with wavelength for these configurations, both measured and modeled, are presented in Figure 7. However, multiple dispersers exhibit tails that extend much further. The primary contributor to the presence of this higher percentage of leakage appears to be whether there is any signal on SCA492. This SCA typically seems to experience a higher parasitic signal contribution to the signal than 491. Consequently, the leakage distributions for dispersers which require the second SCA typically extends to higher values. Additionally, there seems to be a general increase in its imp

**Table 3: Averages and measures of spread for ‘H’ grating configurations, before (BM) and after (AM) applying masking. The 95<sup>th</sup> percentile is given after masking. All values are background as a percentage of signal. The asterisked G395H row contains the statistics obtained when the configuration is cut off at 4.5 $\mu$ m.**

Disperser	Filter	Mean		Median		Standard Deviation		MAD		95 <sup>th</sup> Percentile
		BM	AM	BM	AM	BM	AM	BM	AM	
G140H	F070LP	58.29	1.45	1.91	1.39	1660.09	0.42	0.88	0.28	2.26
G140H	F100LP	235.41	2.89	4.45	2.30	38960.76	1.86	3.23	1.21	6.51
G235H	F170LP	754.19	3.70	5.66	3.53	71798.72	2.16	3.97	1.74	7.39
G395H	F290LP	1739.36	5.78	13.54	3.16	333154.33	6.01	12.73	2.53	19.00
G395H*	F290LP	422.04	2.92	4.50	2.01	28317.45	2.54	3.80	1.39	8.29

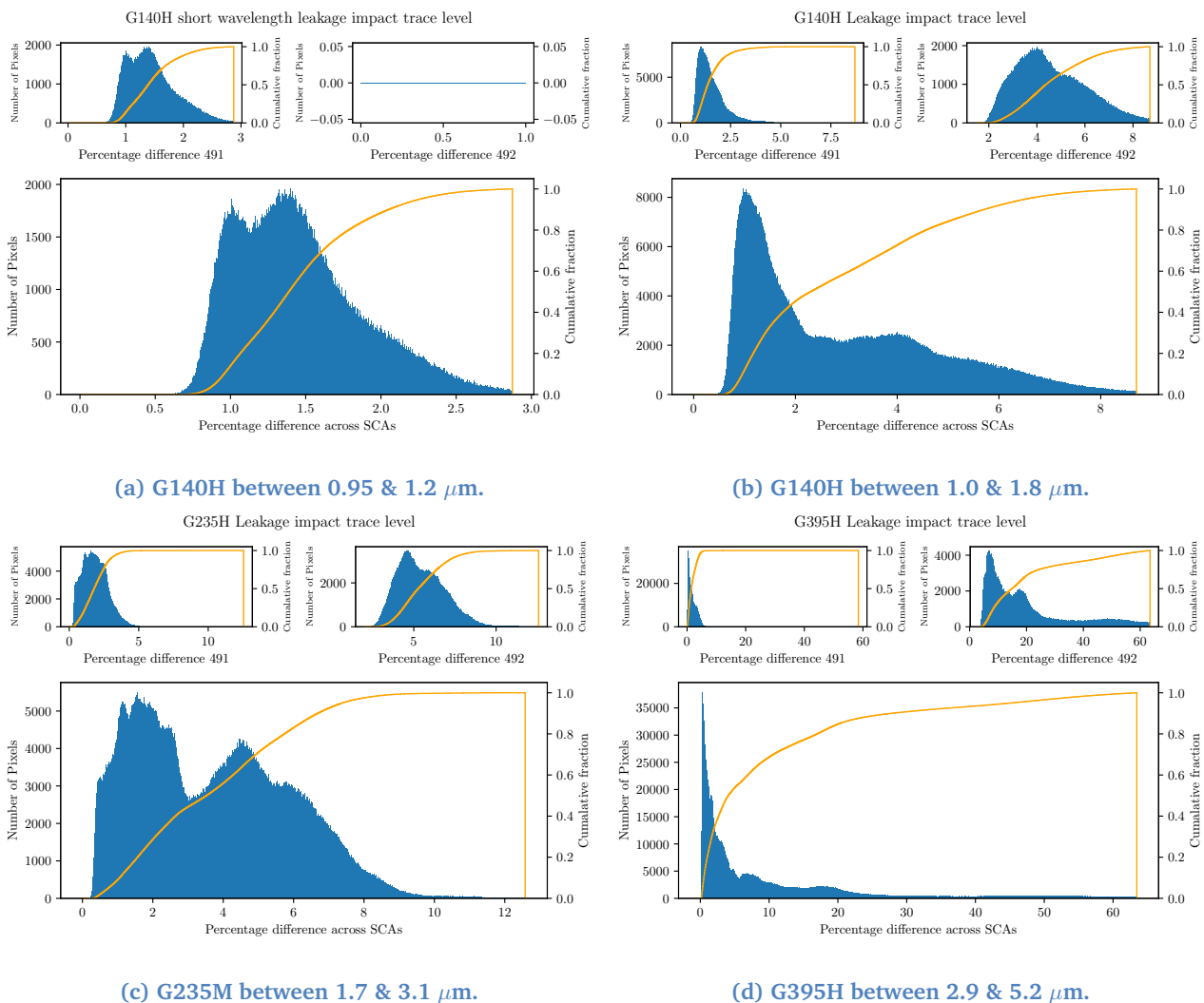
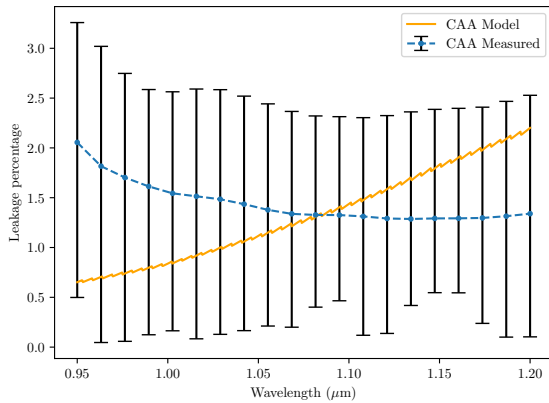


**Figure 6: Histograms showing the distribution of MSA leakage as a percentage of the signal per pixel, for the ‘H’ gratings, in blue. In orange are the cumulative histograms for the same data. In each case 1000 bins were used. The leakage across SCAs 491 and 492 are shown individually, and then together.**

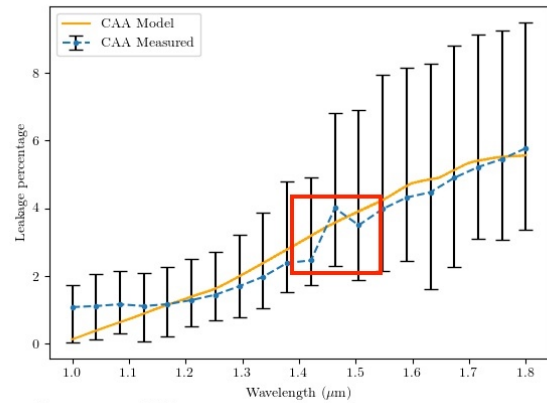
G140H F070LP Leakage Data-Model Comparison



Approx. best contrast: 3500

(a) G140H between 0.95 & 1.23  $\mu\text{m}$ .

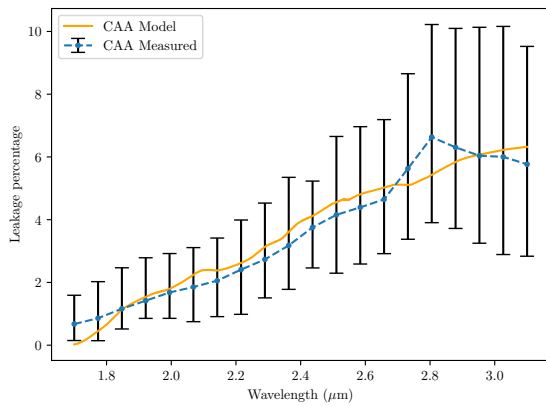
G140H F100LP Leakage Data-Model Comparison



Approx. best contrast: 5500

(b) G140H between 1.0 & 1.8  $\mu\text{m}$ . Red box is SCA gap.

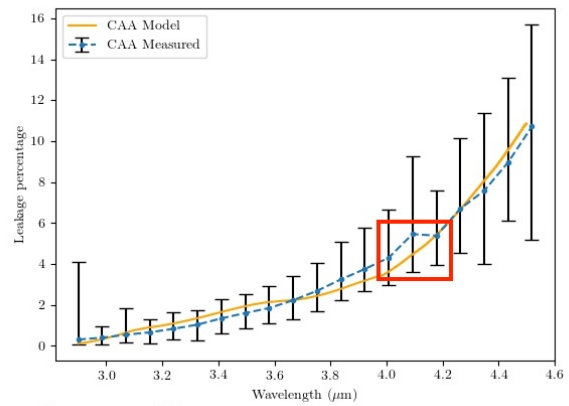
G235H F170LP Leakage Data-Model Comparison



Approx. best contrast: 4000

(c) G235H between 1.7 & 3.1  $\mu\text{m}$ .

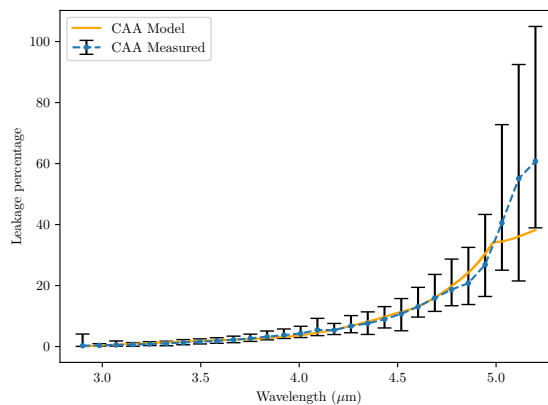
G395H F290LP Leakage Data-Model Comparison



Approx. best contrast: 4000

(d) G395H between 2.9 & 4.5  $\mu\text{m}$ . Red box is SCA gap.

G395H F290LP Leakage Data-Model Comparison



Approx. best contrast: 4000

(e) G395H between 2.9 & 5.2  $\mu\text{m}$ .

Figure 7: Change of the median of leakage as a percentage of signal, with wavelength, for ‘H’ dispersers; observed and modeled. Each scatter plot consists of 20 points, evenly spaced across the individual disperser’s wavelength range. The pseudo error bars, in black, describe the spatial spread of leakage at a wavelength. The lower bound is the minimum value at it, while the upper bound extends to  $3\sigma$  above. The ‘approximate contrast’ refers to the relative contrast used within the model of MOS spectra to IFS spectra.

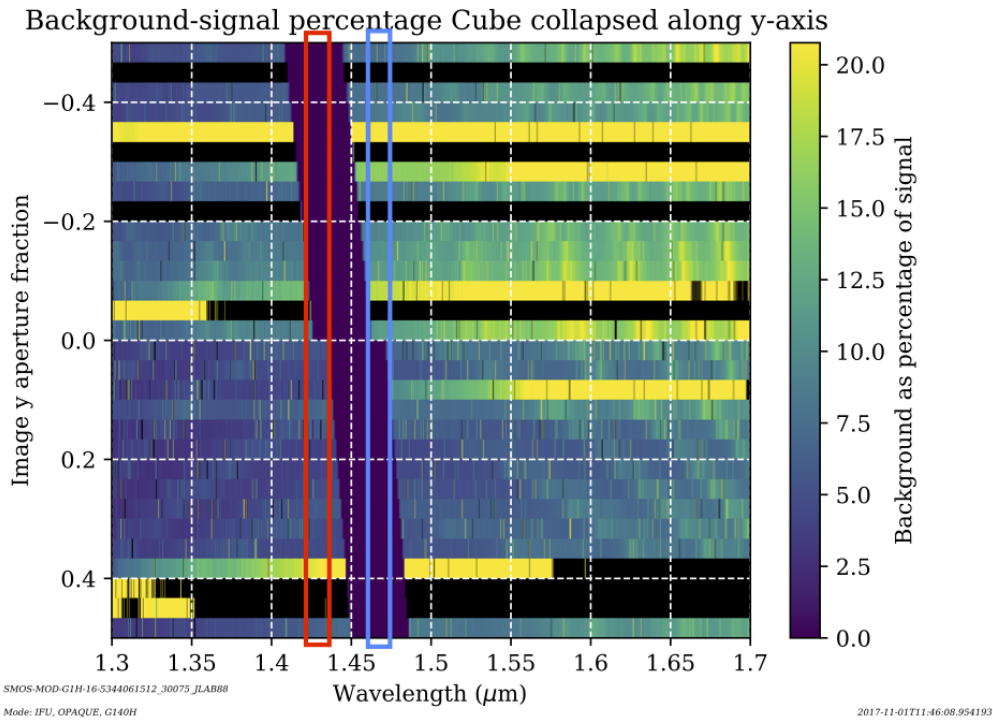


**Figure 8:** Data-cube level illustration of background as a percentage of total signal, for G140H. The cube is viewed collapsed along the y-axis. The red rectangle highlights the wavelength region where only the lower magnitude leakage is available. Whereas the blue rectangle shows the region where only the higher magnitude leakage remains.

-act with wavelength for each disperser. This occurrence, as well as the generally higher percentage on SCA492, can be explained by a combination of two previously discussed factors. Firstly, as with the ‘M’ gratings, the leakage piles up in the detector *i* coordinate. This results in a generally higher level of parasitic signal on SCA492. The second contribution, once more, stems from the shape of the CAA lamp spectra. As previously stated, the spectrum of each lamp drops off at the higher wavelength of each configuration. Again this effect is most pronounced for G395, with statistics provided for G395H both with and without a cut at 4.5 μm. The zeroth order does not fall on the detector for ‘H’ configurations.

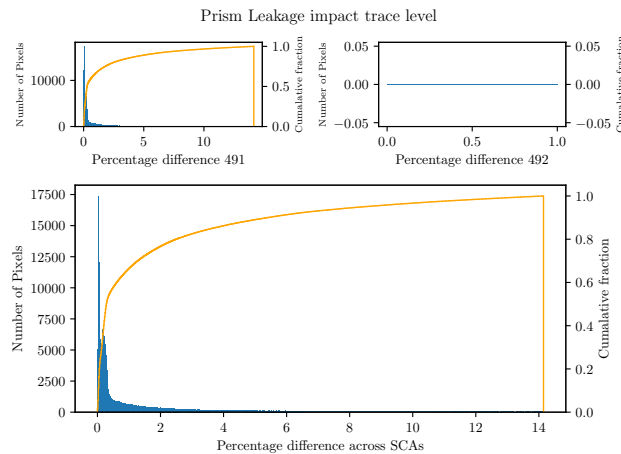
Furthermore, there is a feature to note in Figure 7b. The seemingly oscillatory trend between 1.4 and 1.5 μm can be attributed to the gap between SCAs. This gap is diagonal, in wavelength space. Consequently, when the mean and median is calculated in regions on the gap’s periphery, there is a loss of data that results in lower averages on one side, and higher averages on the other. This occurrence is best seen at the data-cube level, as demonstrated in Figure 8. The effect is also true for G235H, and G395H. However, due to the relatively consistent nature of leakage in G235H at the point in question, the feature is not obvious in Figure 7c. It can, however, be seen for G395H. Finally, modeling discrepancies are explained by the same logic as for ‘M’ results.

### 3.3 The Prism

Finally, the statistics obtained for the Prism, are reported below, in Table 4. The corresponding plots are given in Figure 9. These show the distribution of the parasitic light, and its change in wavelength. For the majority of its wavelength coverage, the Prism suffers from minimal impact from the parasitic signal. In addition, akin to the higher resolution gratings, the Prism does not suffer from the zeroth order problem. The trends observed in Figure 9b are simply effects of the Prism’s spectral resolution.

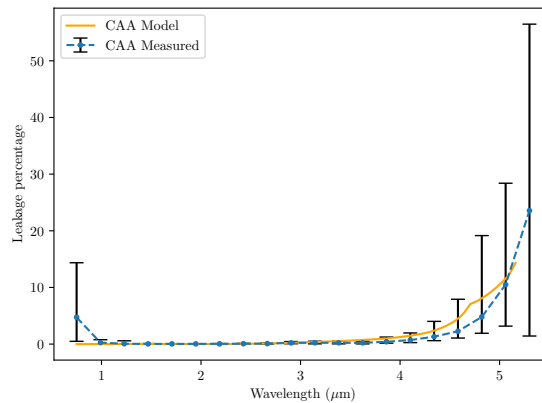
**Table 4: Averages and measures of spread for the Prism, before (BM) and after (AM) applying masking. The 95<sup>th</sup> percentile is given after masking. All values are background as a percentage of signal.**

Disperser	Filter	Mean		Median		Standard Deviation		MAD		95 <sup>th</sup> Percentile
		BM	AM	BM	AM	BM	AM	BM	AM	
PRISM	CLEAR	115.95	1.45	1.10	0.20	11705.43	0.52	1.06	0.15	1.69



**(a) Prism between 0.75 and 5.3  $\mu\text{m}$ . Histogram showing the distribution of MSA leakage as a percentage of the signal per pixel, in blue. In orange is the cumulative histogram for the same data. 1000 bins were used.**

PRISM CLEAR Leakage Data-Model Comparison



Approx. best contrast: 5000

**(b) Prism between 0.75 & 5.3  $\mu\text{m}$ . Change of the median of leakage as a percentage of signal, with wavelength; both observed and modeled. The pseudo error bars, in black, describe the spatial spread of leakage at a given wavelength. The lower bound is the minimum value at that wavelength, while the upper bound extends to  $3\sigma$  above. The ‘approximate contrast’ refers to the relative contrast used within the model of MOS spectra to IFS spectra.**

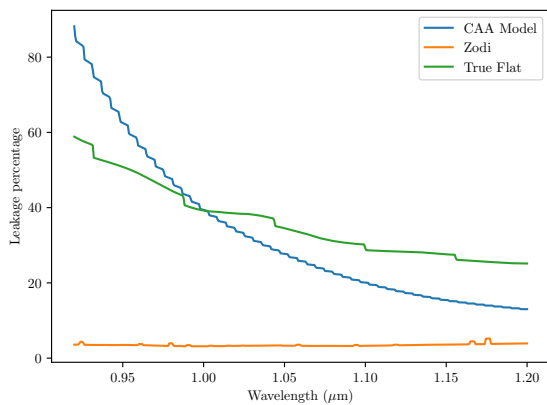
**Figure 9: Quantification of parasitic signal for the Prism disperser, CLEAR filter configuration.**

### 3.4 Simulating the Impact of Zodiacal Light

Once the appropriate contrasts for each instrumental configuration were determined, the relative impact of the parasitic signal for the Zodiacal light could be simulated by feeding it's spectra through the same machinery described in the previous sections. The file used to define the Zodiacal spectrum is 'background\_1.2-zodi\_CL 630\_TOT\_Wm-2m-1arcsec-2.fits'. In the interest of providing points of comparison, a simulation was carried out for a truly flat spectrum as well. This spectrum ranges from 0.4 to 6 microns, with each wavelength assigned a value of  $1 \times 10^{-12} \text{ Wm}^{-2}\text{m}^{-1}\text{arcsec}^{-2}$ . This spectrum is given in the input file 'flatspectrum.py'. The results from these are shown below, in Figure 10.

Carrying out these simulations reveals that the relative importance of the leakage differs significantly between the CAA lamps, and the true Zodiacal spectrum. The most extreme deviations occur for the G140M, and both G395 configurations. In the case of G140M, the impact of the zeroth order is greatly reduced; owing to the fact that the energy distribution of IFS -1 order is stronger on its bluer edge. Consequently, over the relevant wavelength range, the IFS spectrum is much closer in magnitude to the MOS zeroth order than in the case of the CAA lamps. On the other hand, the differences for the G395 gratings are simply due to the fact that the Zodiacal spectrum extends well beyond the science range of these configurations, whereas the spectrum for FLAT 3 drops off rapidly towards its upper bound. Similarly, for the remaining configurations, the generally heightened levels of leakage can be explained by the greater extent and more balanced nature of the Zodiacal spectrum. From the model, 95<sup>th</sup> percentiles for the Zodiacal light were also obtained. These are provided below

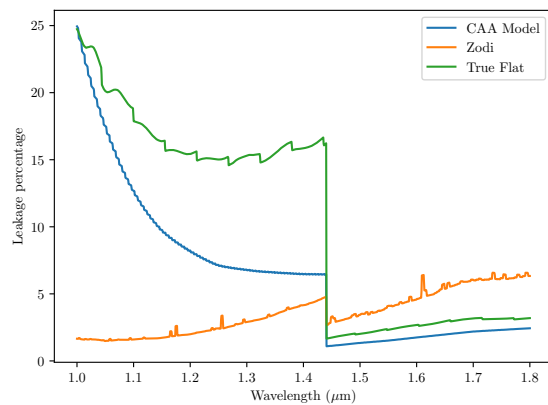
G140M F070LP Modeled Source Comparison



Approx. best contrast: 3500

(a) G140M between 0.95 & 1.23 μm.

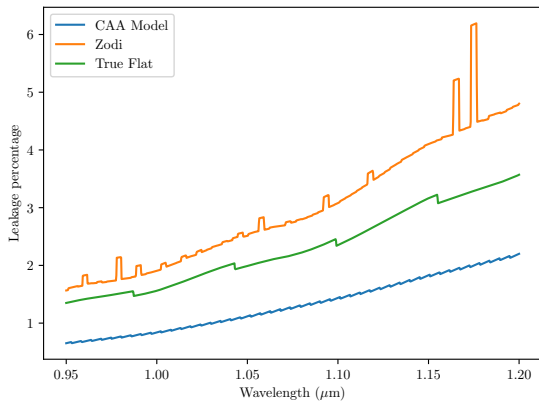
G140M F100LP Modeled Source Comparison



Approx. best contrast: 5500

(b) G140M between 1.0 & 1.8 μm.

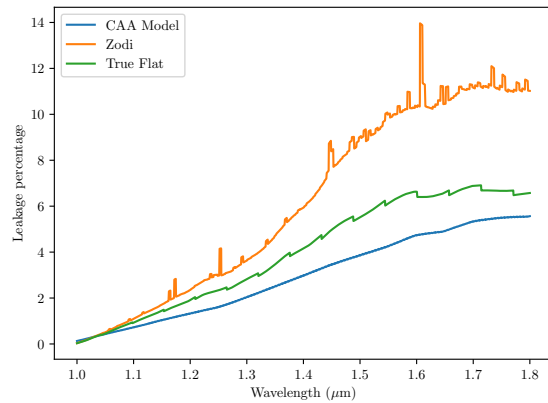
G140H F070LP Modeled Source Comparison



Approx. best contrast: 3500

(c) G140H between 0.95 & 1.23 μm.

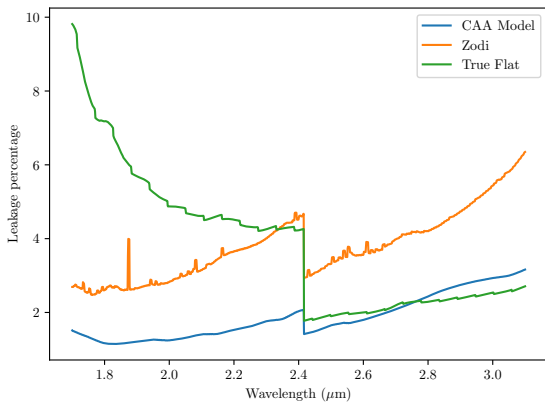
G140H F100LP Modeled Source Comparison



Approx. best contrast: 5500

(d) G140H between 1.0 & 1.8 μm.

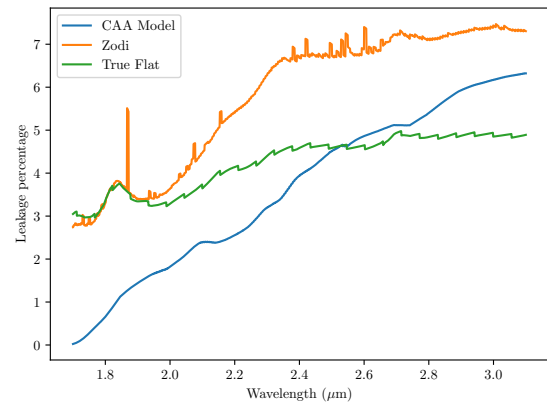
G235M F170LP Modeled Source Comparison



Approx. best contrast: 4000

(e) G235M between 1.7 & 3.1  $\mu\text{m}$ .

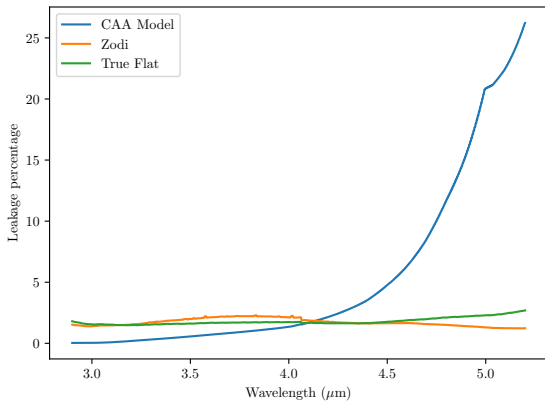
G235H F170LP Modeled Source Comparison



Approx. best contrast: 4000

(f) G235H between 1.7 & 3.1  $\mu\text{m}$ .

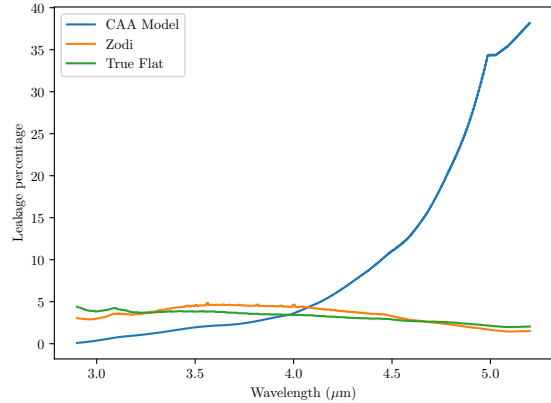
G395M F290LP Modeled Source Comparison



Approx. best contrast: 4000

(g) G395M between 2.9 & 5.2  $\mu\text{m}$ .

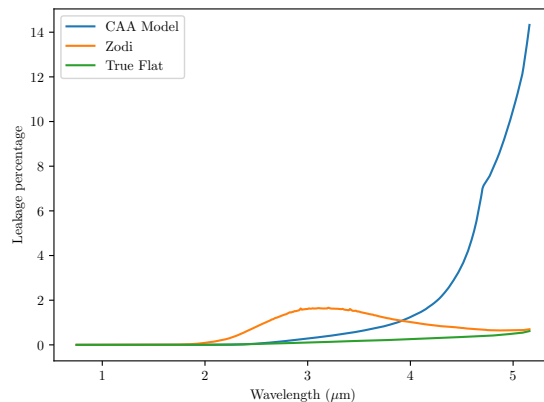
G395H F290LP Modeled Source Comparison



Approx. best contrast: 4000

(h) G395H between 2.9 & 5.2  $\mu\text{m}$ .

PRISM CLEAR Modeled Source Comparison



Approx. best contrast: 5000

(i) Prism between 0.75 & 5.3  $\mu\text{m}$ .

Figure 10: Simulated levels of 'leakage' from the 1D model. Relative levels of MOS signal to IFS signal are shown for the CAA lamps, Zodiacal light, and a truly flat spectrum for each possible instrumental configuration. The 'approximate contrast' refers to the relative contrast used within the model of MOS spectra to IFS spectra.

**Table 5: Corrected 95<sup>th</sup> percentiles of relative MSA leakage for the modeled Zodiacal light, together with the contrast of each configuration determined using the model. Percentile values are the background as a percentage of IFS signal.**

Disperser	Filter	95 <sup>th</sup> Percentile	Approx. Contrast
G140M	F070LP	3.91	3500
G140M	F100LP	6.22	5500
G140H	F070LP	4.70	3500
G140H	F100LP	11.29	5500
G235M	F170LP	5.67	4000
G235H	F170LP	7.37	4000
G395M	F290LP	2.22	4000
G395H	F290LP	4.62	4000
PRISM	CLEAR	1.63	5000

in Table 5, alongside the estimated contrast of the configuration.

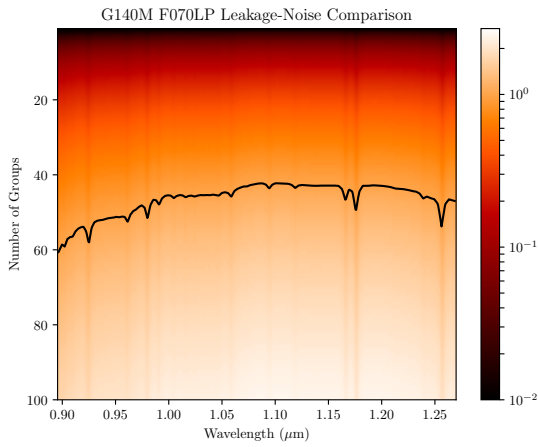
#### 4 EVALUATING THE IMPACT ON AN OBSERVATION

Having quantified the impact of the parasitic signal, we considered how it compares to Zodiacal background, from an observational perspective. The analysis conducted in Section 3 gives us important quantitative information on how the leakage background level compares to the observed spectrum of the incident background. It is, however, difficult for an observer to use these metrics to directly evaluate the impact of the MSA leakage on a specific observation. A much better metric for this purpose is how the leakage level compares to the  $1\sigma$  noise level of an integration of the extended background source causing it. This metric can easily be scaled for an observation composed of multiple integrations, and the results can be compared to the signal-to-noise ratio (SNR) expected for the scientific target itself.

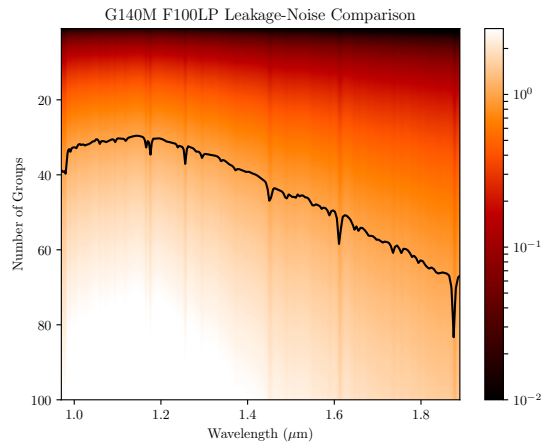
Given that this component is typically a small percentage of the Zodiacal light, in a single image the total noise of the exposure may be the dominant concern for an observer. However, an integration is made up of multiple groups; themselves made from multiple frames. As the number of groups is increased, the SNR of the exposure increases. This results in an important consideration for background subtraction; the impact of the MSA leakage will grow with the SNR, and eventually it will become comparable to the impact of the total noise. For the purpose of charting this growth, the JWST Exposure Time Calculator (ETC), the Pandeia Engine, was used. To model the spectrum of the Zodiacal light, its spectrum was defined using the file ‘background\_1.2-zodi\_CL630\_TOT\_MJysr-1.fits’.

Initially, this file was used to satisfy the ‘background’ parameter within the Pandeia engine. Then, as a conservative estimate of the MSA leakage, the 95<sup>th</sup> percentile result, stated in Table 5, for each configuration was applied as a factor for each file. This modified file was, separately for each configuration, used as the ‘object’ to put into the ETC. In this way, the ETC’s SNR calculation functionality could be used to determine how the parasitic signal compares to the total noise for an exposure, when Zodiacal light is an observational background.

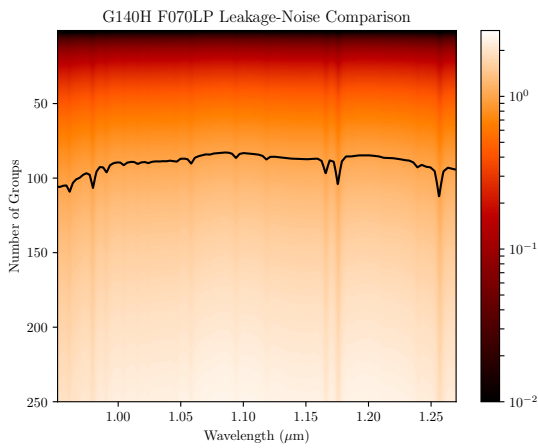
The ETC was configured to use the detector readout mode ‘NRSIRS2RAPID’. This process was repeated progressively increasing the number of groups used in an integration. From this, heat-maps were generated displaying how the ratio of parasitic signal to the total noise changes across its spectrum, and with the number of groups used. A contour was also overlaid on these plots highlighting when the ratio between the leakage signal and noise reached 1.0. The resulting heat-maps are presented below, in Figure 11.



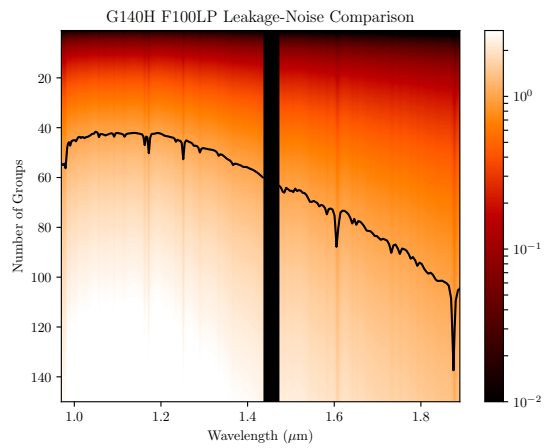
(a) G140M using FLAT4.



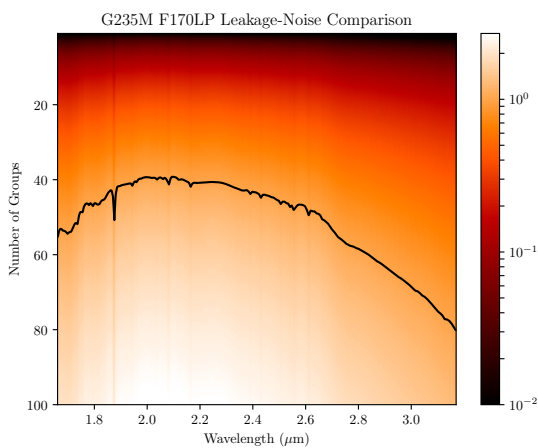
(b) G140M using FLAT1.



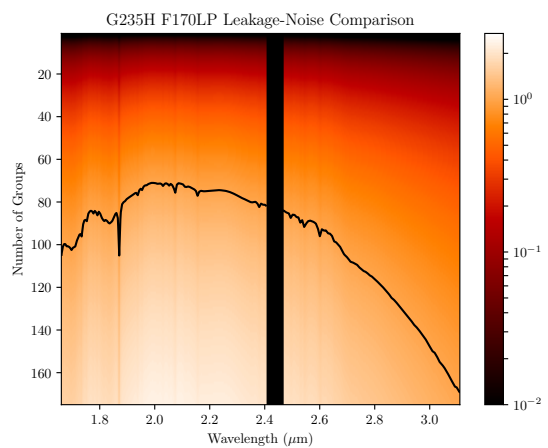
(c) G140H using FLAT4.



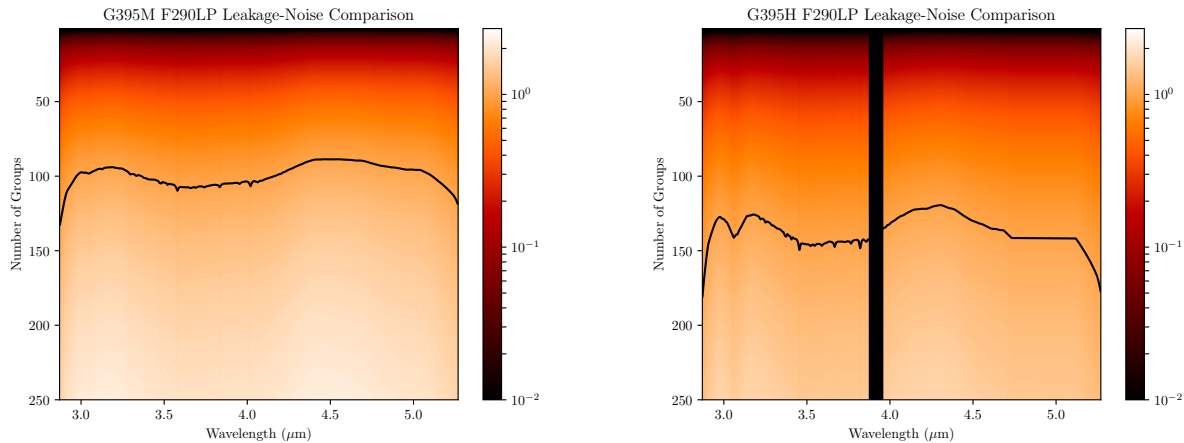
(d) G140H using FLAT1.



(e) G235M using FLAT2.

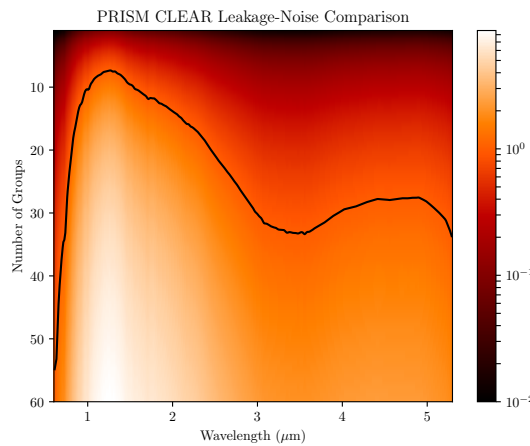


(f) G235H using FLAT2.



(g) G395M using FLAT3. From data up to 5.2  $\mu\text{m}$ .

(h) G395H using FLAT3. From data up to 5.2  $\mu\text{m}$ .



(i) Prism using FLAT5.

Figure 11: Heat-maps showing the ratio between the parasitic leakage signal and the total noise for an exposure of Zodiacal light, as it changes across the spectrum of the Zodiacal light and with the number of groups included in an exposure. The black-lines demarcate the contour where this ratio reaches 1.0.

## 5 CONCLUSION

This investigation set out to study, qualitatively and quantitatively, the effect on the MSA leakage on observations with the IFU. Statistical analysis was carried out on test data generated using the Calibration Assembly. While three different data pipeline levels were explored, the 2D irregular spectrum stage was determined to be ideal for this analysis. The impact of the parasitic signal was specifically quantified by calculating what percentage of the total signal it made up.

Masking was carried out to exclude the impact of FO shutters and bad pixels. Histograms were generated showing the distribution of the leakage signal for the various configurations of the instrument. From these it was found that the majority of it is < 10% of the signal. However, with a tail of data that typically extends much further. The impact of the leakage was found to be repeatedly higher on SCA492, and this appeared to be the greatest contributor to the higher magnitude tails. The means, medians, standard deviations, and MADs of each of these data sets were calculated; both before and after masking. The 95<sup>th</sup> percentile, after masking, was also calculated. Additionally, a rudimentary, 1D model of the parasitic signal was constructed in order to compare

the leakage from different sources. Consequently, an estimated 95<sup>th</sup> percentile value was also obtained for leakage due to the Zodiacal light. This quantity was used as a conservative metric for comparing how the parasitic signal compares to Zodiacal light, and charting how this relationship evolves with the number of groups used in an integration.

In addition to this work, there still remains further scope for better understanding the MSA leakage. Work needs to be done in exploring how the precise structure of the leakage changes after rotations of NIRSpec's grating wheel. Furthermore, there is need to explore how this impact compares to other sources of noise or background, as well as understand in what regimes precise leakage subtraction is required. Finally, work must be carried out to develop the model of the leakage into a more comprehensive one. The reason behind the additional factor necessitated in zeroth order cases needs to be identified, and a robust fitting regime needs to be used to obtain precise contrast values across configurations.

## 6 REFERENCES

- Dorner, B. 2012, Verification and science simulations with the Instrument Performance Simulator for JWST/NIRSpec, Phd thesis, Universite de Lyon
- Giardino, G. 2013, An introduction to the NIRSpec parametric model, Technical Note NTN-2013-011, ESTEC
- Iglewicz, B. & Hoaglin, D. 1993, The ASQC Basic References in Quality Control: Statistical Techniques, Vol. 16, How to Detect and Handle Outliers (ASQC Quality Press)
- Lützgendorf, N. 2017, Tracing the MSA leakage component common to all shutters, Technical Note ESA-JWST-SCI-NRS-TN-2017-051, STScI